RSC Advances

PAPER

View Article Online
View Journal | View Issue

Check for updates

Cite this: *RSC Adv.*, 2019, **9**, 19126

Microwave-assisted synthesis of mutually embedded Rh concave nanocubes with enhanced electrocatalytic activity†

Junxuan Xu, Hongbin Tang, Baogui Ning, Yanxi Zhao and Tao Huang *

Received 9th April 2019
Accepted 12th June 2019

DOI: 10.1039/c9ra02650a

rsc.li/rsc-advances

Novel mutually embedded Rh concave nanocubes were synthesized by reducing $Rh(acac)_3$ in tetraethylene glycol in the presence of benzyldimethylhexadecylammonium, KI and polyvinylpyrrolidone under microwave irradiation for 120 s. KI and HDBAC were crucial to the formation of mutually embedded nanostructures. The as-prepared Rh nanocrystals exhibited higher electrocatalytic activity and stability.

Open Access Article. Published on 18 June 2019. Downloaded on 5/2/2026 7:02:40 AM.
This article is licensed under a Creative Commons Attribution-NonCommercial 3.0 Unported Licence.

As important catalytic materials, the controlled syntheses of platinum group metal nanocatalysts have attracted wide attention for many years. The catalytic performances of platinum group metal nanomaterials are highly dependent upon their morphologies, compositions and surface structures. Their nanocrystals with controlled shapes have been extensively explored in order to promote their catalytic performance and reduce their cost because of their scarcity and high prices. As an important platinum group metal, rhodium (Rh) is often used as a typical catalyst with high activity and selectivity in hydroreduction,[1] hydroformylation,[1f,2] NO_x reduction,[3] CO oxidation,[4] cross coupling,[5] and fuel cell[1g,4d,6] and other chemical reactions.[7] In addition, Rh has a strong resistance to acids and bases as well as a high melting point. However, nanoscaled Rh exhibits high thermodynamic instability owing to its high surface free energy, although it is more stable than many other catalytically active metals. So, the shape-controlled synthesis of Rh nanocrystals is still one of the challenges in this field, though Pt and Pd nanocrystals with many different morphologies have been obtained. In the past decade, great efforts have been devoted to tailoring the sizes, morphologies and surface structures of Rh nanoparticles to improve their catalytic efficiency because of the scarcity and preciousness. Up to now, many Rh nanomaterials with various morphologies such as nanosheets,[1f,4a,8] nanotetropods,[9] hierarchical dendrites,[6] hyperbranched nanoplates,[1g,10] ultrathin nanosheet assemblies,[1e,7a] and cubic,[11] tetrahedral,[1d] icosahedral,[12] tetrahexahedral,[4d] concave cubic,[13] concave tetrahedral nanocrystals,[14] as well as cubic nanoframes,[5b,5c] truncated octahedral nanoframes,[15] multipods[16] and mesoporous[3] Rh nanoparticles have been successfully synthesized. Moreover, all the obtained Rh nanoparticles were monodispersed and displayed enhanced catalytic activities. Although various nanoparticles with concave, frame, branched, or hierarchical structures as well as normal flat or convex surfaces have been created, it is still worthy to develop further novel Rh nanostructures.

Herein, we report a facile microwave-assisted strategy for a one-pot synthesis of mutually embedded Rh concave nanocubes, a unique hierarchical nanostructure with several identical concave nanocubes embedded in each other. The co-adsorption of I^- ions and benzyldimethylhexadecylammonium (HDBAC) was dominantly responsible for the generation of the hierarchical concave cubic Rh nanocrystals. The as-prepared Rh nanocrystals displayed an enhanced electrochemical activity for formic acid electro-oxidation.

Fig. 1a and b as well as Fig. S1 (ESI†) display TEM images of the typical Rh nanocrystals synthesized under microwave irradiation for 120 s in the presence of PVP and an appropriate amount of KI and HDBAC. Interestingly, as can be seen, the resulting Rh nanocrystals were present in mutually embedded concave nanocubic morphologies under TEM, showing a unique hierarchical nanostructure feature. This hierarchical structure was consisted of at least two concave cubes (Fig. 1b) which were embedded in each other. If considering an individual concave nanocube, the average diameter was about 85 nm. The high-resolution TEM image, as shown in Fig. 1c and d, showed the lattice fringes with an interplanar spacing of 0.192 and 0.135 nm, which can be indexed to the (200) and (220) planes of face-centered cubic (fcc) Rh. The corresponding fast Fourier transform (FFT) pattern for the selected box area in Fig. 1c is shown in the inset in Fig. 1d, indicating a single crystal structure and good crystallinity. In fact, the as-prepared concave cube demonstrated octapod characteristics because of its showing both concave faces and concave edges. The SEM image further confirmed hierarchical structure feature. As shown in Fig. 1e and the inset for partially enlarged picture as well as Fig. S2 (ESI†), the concave nanocubic structures and their mutually embedded feature are present clearly.

College of Chemistry and Material Science, South-Central University for Nationalities, Wuhan 430074, China. E-mail: huangt208@163.com

† Electronic supplementary information (ESI) available: TEM and SEM images. See DOI: 10.1039/c9ra02650a

This journal is © The Royal Society of Chemistry 2019

Open Access Article. Published on 18 June 2019. Downloaded on 5/2/2026 7:02:40 AM.
This article is licensed under a Creative Commons Attribution-NonCommercial 3.0 Unported Licence.

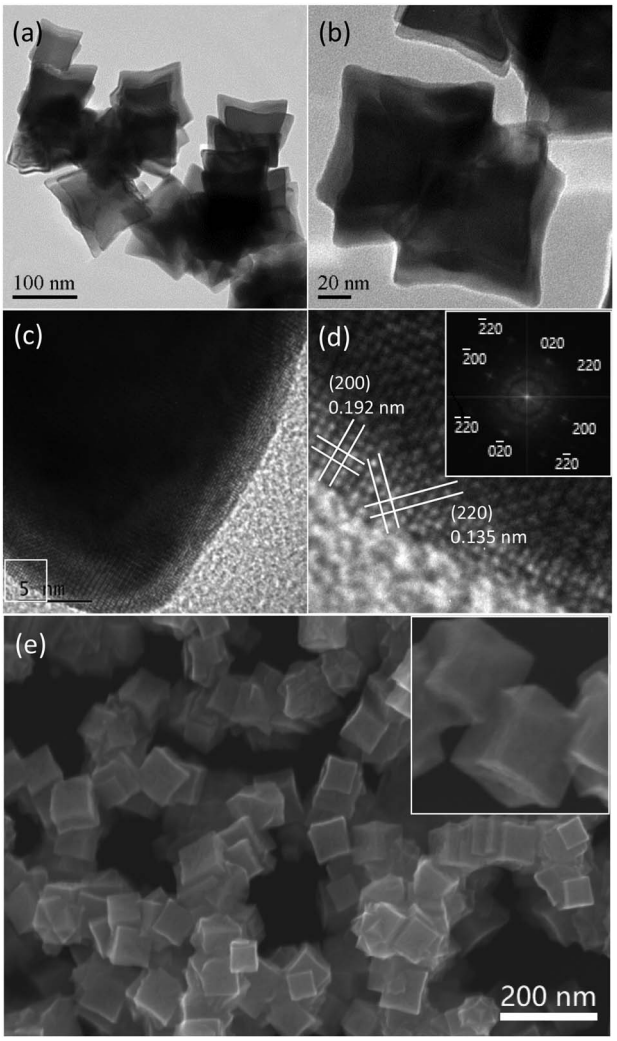

Fig. 1 TEM (a and b), HRTEM (c and d) and SEM (e) images of the as-prepared mutually embedded Rh concave nanocubes. (d) shows the selected box area in (c). The insets in (d and e) show the FFT pattern and a partially enlarged SEM picture, respectively.

The typical XRD pattern of the as-synthesized mutually embedded Rh concave nanocubes is shown in Fig. 2. The characteristic peaks at 41.28, 48.05, 70.18 and 84.45° are corresponding well with the (111), (200), (220) and (311) lattice planes according to the standard diffraction file (JCPDS 05-0685), respectively. The sharp and strong (111) diffraction peak, which indicated the preferential orientation of (111) planes and the consistency with the HRTEM observation, suggested its high purity and crystallinity of the obtained Rh nanocrystals. In addition, XPS measurement demonstrated the binding energy of Rh $3d_{5/2}$ and Rh $3d_{3/2}$ at 307.16 and 311.91 eV (Fig. 3), respectively, with an interval of 4.75 eV, which was coincident with the reference values (307.0 and 311.75 eV),[17] indicating Rh^0 with zero oxidation for the as-prepared mutually embedded concave nanocubes.

It was worth noting that the use of KI was much essential for creating the mutually embedded Rh concave nanocubes. As shown in Fig. 4a, except flower ball structures connected with

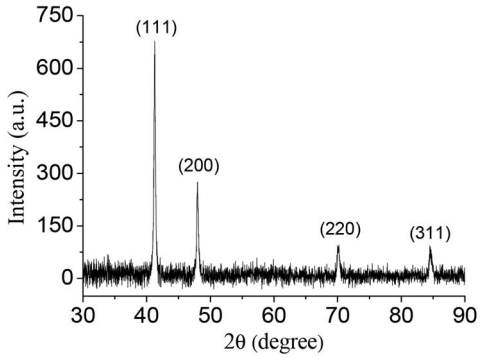

Fig. 2 XRD pattern of the typical mutually embedded Rh concave nanocubes.

each other, neither concave cube nor hierarchical structure was observed in the absence of KI. When 0.4 mmol of KI was added, the embedded Rh concave nanocubes accompanying with some irregular nanostructures were generated (Fig. 4b). With further increasing the amount of KI from 0.8 to 1.2 mmol, complex inter-embedded nanostructures with obscure polyhedral outlines were formed (Fig. 4c and d). Accordingly, an excessive amount of KI was unfavorable for the generation of the mutually embedded Rh concave nanocubes. According to the previous report,[18] the addition of KI would manipulate the reducing kinetics to generate Rh concave nanostructures under microwave irradiation. In the presence of KI, the precursor was transformed to a more stably coordinated anion $[RhI_6]^{3-}$. As a result, the reducing rate of Rh(III) to Rh(0) as well as both the nucleation and growth rate of Rh nanoparticles decreased, which would be favorable for the oriented growth of Rh concave cubes. The role of I^- ions was elucidated by using an equivalent amount of KBr or KCl in stead of KI, respectively, under the same other conditions. As can be seen (Fig. S3, ESI†), no single or embedded concave nanocubes but amorphous Rh nanoparticles with agglomeration were observed under these two alternative experiments. These results suggested that different halides would result in different Rh nanostructures and the existence of an appropriate amount of I^- ions was beneficial for the formation of the mutually embedded Rh concave

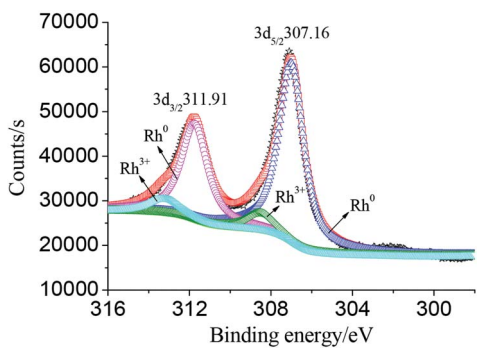

Fig. 3 XPS spectrogram of the typical mutually embedded Rh concave nanocubes.

Open Access Article. Published on 18 June 2019. Downloaded on 5/2/2026 7:02:40 AM.
This article is licensed under a Creative Commons Attribution-NonCommercial 3.0 Unported Licence.

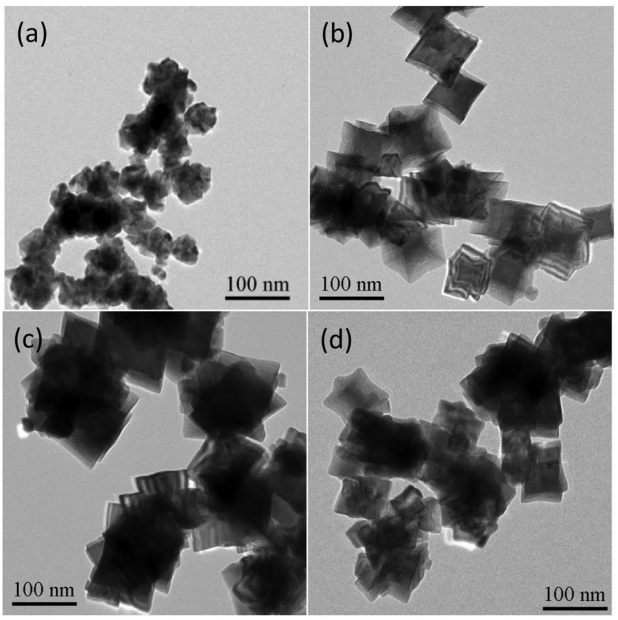

Fig. 4 TEM images of the products prepared with different amount of KI while keeping the same other conditions. (a) Without KI; (b) 0.4 mmol KI; (c) 1.2 mmol KI; (d) 1.6 mmol KI.

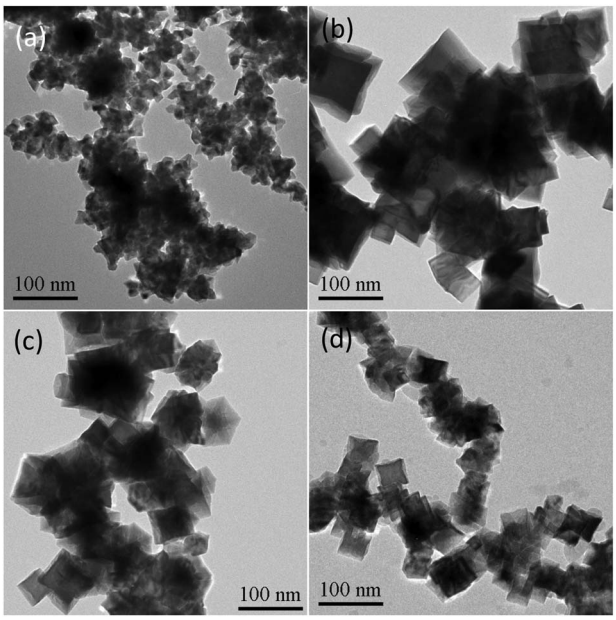

Fig. 5 TEM images of the products prepared with different amount of HDBAC while keeping the same other conditions. (a) Without HDBAC; (b) 0.1 mmol HDBAC; (c) 0.4 mmol HDBAC; (d) 0.6 mmol HDBAC.

nanocubes. According to the literature,[19] halides tend to selectively adsorb to {100} planes. Generally, the six surfaces of a Rh cube are ⟨100⟩ oriented. So, we suggested that the selective adsorption of I^- ions on Rh {100} planes confined a growth along ⟨100⟩ direction and facilitated the formation of Rh concave structures with growth along {111} facets.

Moreover, the effect of HDBAC on the creation of the embedded Rh concave nanocubes was also investigated. As shown in Fig. 5a, no shaped Rh nanocrystal was produced except agglomerated nanoparticles without using HDBAC. While 0.1 mmol of HDBAC was used relatively to the parameters in the typical experimental procedure, Rh nanostructures with an nonuniform cross-sectional dimension and overly embedded each other were generated (Fig. 5b). With further increasing the amount of HDBAC from 0.4 to 0.6 mmol, the cross-section dimension and the concavity of the concave Rh nanocubes decreased gradually though embedded Rh nanostructures were still generated (Fig. 5c and d). Whereas no concave nanostructure was observed with using an equivalent amount of CTAB or CTAC in stead of HDBAC, respectively (Fig. S4, ESI†). These results implied that the formation as well as the size and surface structure of the mutually embedded Rh concave nanocubes were dependent upon the confinement effect of HDBAC. On the one hand, the existence of HDBAC would contribute to creation of the concave cubes and their mutually embedded structures, on the other hand, the growth of shaped Rh nanoparticles was confined and the adsorption of I^- ions on Rh {100} planes was disturbed, resulting in less concavity and smaller size, due to an excessive amount of HDBAC.

In order to investigate whether its formation was related to oxidation etching of Rh surface by I^- ion/O_2,[19,20] nitrogen was filled into the reaction bottle to remove oxygen before reaction and the same results were obtained. So, the oxidative etching can be negligible, which may be ascribed to the extremely short time under microwave irradiation.

According to the previous report,[21] based on the results of the experiments with dependent I^- ions and HDBAC, the formation of the mutually embedded Rh concave nanocubes may be ascribed to symmetry breaking due to asymmetric passivation and attachment of Rh nuclei. I^- ions were responsible for retarding the growth of {100} and {110} facets of cubic nuclei and promoting the preferential overgrowth on {111} planes, resulting in the formation of the concave structure with concave faces and edges. However, the existence of an appropriate amount of HDBAC may retard the deposition of Rh atoms on one or two corners with (111) facets due to the confinement, resulting in symmetry breaking. Meanwhile, with the confinement of HDBAC, the inevitable collision of nuclei leads to attachment of nuclei one another along the confined corners due to surface defects or dislocations. As a result, the mutually embedded Rh concave nanocubes would be generated with the growth of nuclei.

The electrochemical performances of the as-synthesized Rh nanocrystals were examined by electrocatalytic oxidation of formic acid. The specific current density was normalized to the electrochemical surface area (ECSA). According to the cyclic voltammetry (CV) curves (Fig. S5†), the ECSAs were calculated as 66.5 and 52.3 $m^2\ g^{-1}$ for the mutually embedded Rh concave nanocubes and the commercial Rh black, respectively. Fig. 6a shows the CV curves for the electro-oxidation of formic acid in $HClO_4$ by the as-prepared mutually embedded Rh concave nanocubes and the commercial Rh black. The peak current density for the mutually embedded Rh concave nanocubes was

 This journal is © The Royal Society of Chemistry 2019

Open Access Article. Published on 18 June 2019. Downloaded on 5/2/2026 7:02:40 AM.
This article is licensed under a Creative Commons Attribution-NonCommercial 3.0 Unported Licence.

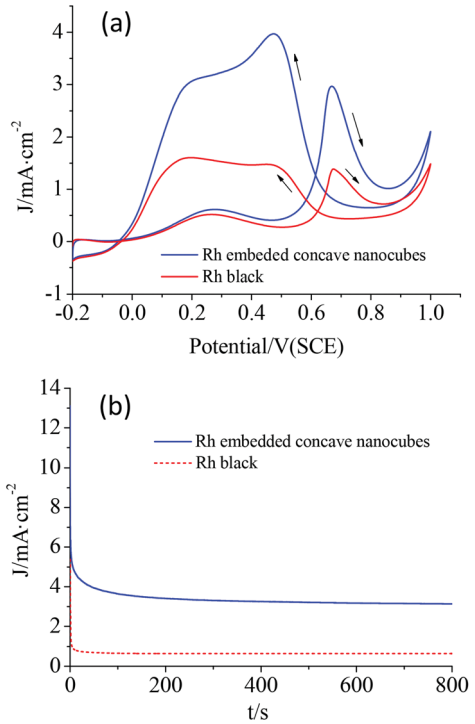

Fig. 6 The CV (a) and CA (b) curves of the mutually embedded Rh concave nanocubes and Rh black in 0.1 M $HClO_4$ + 0.5 M HCOOH solutions with the cyclic potential between −0.2 and 1.0 V at a sweep rate of 50 mV s^{-1}.

measured to be 2.988 mA cm^{-2} at 0.667 V, while it was 1.379 mA cm^{-2} at 0.674 V for Rh black. The electrocatalytic activity of the hierarchical Rh nanostructures, though with a larger size, was about 2.2 times that of Rh black. Obviously, the mutually embedded Rh concave nanocubes exhibited an enhanced electrocatalytic activity for formic acid comparing with the commercial Rh black, which should be ascribed to their special surface structure with more edges, corners and terraces. Fig. 6b shows the CA curves of the electrocatalytic oxidation of formic acid for these catalysts. Compared with Rh black, a slower current attenuation as well as a higher retention of current after 800 s was observed for the as-prepared embedded Rh concave nanocubes, revealing a good electrochemical stability.

In summary, a novel hierarchical Rh nanostructure with several concave nanocubes embedded mutually could be rapidly prepared by reducing $Rh(acac)_3$ in TEG under microwave irradiation for 120 s in the presence of PVP and an appropriate amount of KI and HDBAC. In the preparing process, TEG was used as both a solvent and a reducing agent. The existence of KI and HDBAC was critical to the formation of the mutually embedded Rh concave nanocubes. The as-prepared mutually embedded Rh concave nanocubes demonstrated higher electrocatalytic activity and stability than commercial Rh black in the electro-oxidation of formic acid.

Conflicts of interest

There are no conflicts to declare.

Acknowledgements

This work was supported by the National Nature Science Foundation of China (Grant 21273289).

Notes and references

1 (*a*) X. D. Mu, J. X. Meng, Z. C. Li and Y. Kou, *J. Am. Chem. Soc.*, 2005, **127**, 9694–9695; (*b*) R. R. Dykeman, N. Yan, R. Scopelliti and P. J. Dyson, *Inorg. Chem.*, 2011, **50**, 717–719; (*c*) X. Y. Quek, Y. J. Guan and E. J. M. Hensen, *Catal. Today*, 2012, **183**, 72–78; (*d*) K. H. Park, K. Jang, H. J. Kim and S. U. Son, *Angew. Chem., Int. Ed.*, 2007, **46**, 1152–1155; (*e*) Y. Jiang, J. Su, Y. Yang, Y. Jia, Q. Chen, Z. Xie and L. Zheng, *Nano Res.*, 2016, **9**, 849–856; (*f*) H. Duan, N. Yan, R. Yu, C.-R. Chang, G. Zhou, H.-S. Hu, H. Rong, Z. Niu, J. Mao, H. Asakura, T. Tanaka, P. J. Dyson, J. Li and Y. Li, *Nat. Commun.*, 2014, **5**, 3093–3100; (*g*) J. Zhang, M. Chen, J. Chen, H. Li, S. Wang, Q. Kuang, Z. Cao and Z. Xie, *Sci. China Mater.*, 2017, **60**, 685–696.

2 (*a*) R. Franke, D. Selent and A. Börner, *Chem. Rev.*, 2012, **112**, 5675–5732; (*b*) C. Hou, G. F. Zhao, Y. J. Ji, Z. Q. Niu, D. S. Wang and Y. D. Li, *Nano Res.*, 2014, **7**, 1364–1369; (*c*) Y. Yuan, N. Yan and P. J. Dyson, *ACS Catal.*, 2012, **2**, 1057–1069; (*d*) Z. Sun, Y. H. Wang, M. M. Niu, H. Q. Yi, J. Y. Jiang and Z. L. Jin, *Catal. Commun.*, 2012, **27**, 78–82; (*e*) S. Xie, X. Y. Liu and Y. Xia, *Nano Res.*, 2015, **8**, 82–96.

3 B. Jiang, C. Li, O. Dag, H. Abe, T. Takei, T. Imai, M. S. A. Hossain, M. T. Islam, K. Wood, J. Henzie and Y. Yamauchi, *Nat. Commun.*, 2017, **8**, 15581.

4 (*a*) C. Hou, J. Zhu, C. Liu, X. Wang, Q. Kuang and L. Zheng, *CrystEngComm*, 2013, **15**, 6127–6130; (*b*) Y. W. Zhang, M. E. Grass, W. Y. Huang and G. A. Somorjai, *Langmuir*, 2010, **26**, 16463–16468; (*c*) M. E. Grass, Y. W. Zhang, D. R. Butcher, J. Y. Park, Y. M. Li, H. Bluhm, K. M. Bratlie, T. F. Zhang and G. A. Somorjai, *Angew. Chem., Int. Ed.*, 2008, **47**, 8893–8896; (*d*) N. F. Yu, N. Tian, Z. Y. Zhou, L. Huang, J. Xiao, Y. H. Wen and S. G. Sun, *Angew. Chem., Int. Ed.*, 2014, **53**, 5097–5101.

5 (*a*) V. K. Kanuru, S. M. Humphrey, J. M. W. Kyffin, D. A. Jefferson, J. W. Burton, M. Armbruster and R. M. Lambert, *Dalton Trans.*, 2009, **37**, 7602–7605; (*b*) S. Xie, N. Lu, Z. Xie, J. Wang, M. J. Kim and Y. Xia, *Angew. Chem., Int. Ed.*, 2012, **51**, 10266–10270; (*c*) W. Ye, S. Kou, X. Guo, F. Xie, H. Sun, H. Lu and J. Yang, *Nanoscale*, 2015, **7**, 9558–9562.

6 Y. Kang, F. Li, S. Li, P. Jin, J. Zeng, J. Jiang and Y. Chen, *Nano Res.*, 2016, **9**, 3893–3902.

7 (*a*) J. Bai, G.-R. Xu, S.-Hi Xing, J.-H. Zeng, J.-X. Jiang and Y. Chen, *ACS Appl. Mater. Interfaces*, 2016, **8**, 33635–33641; (*b*) H. M. Liu, S. H. Han, Y. Zhao, Y. Y. Zhu, X. L. Tian, J. H. Zeng, J. X. Jiang, B. Y. Xia and Y. Chen, *J. Mater. Chem. A*, 2018, **6**, 3211–3217; (*c*) J. Du, X. Wang, C. Li, X. Y. Liu, L. Gu and H. P. Liang, *Electrochim. Acta*, 2018, **282**, 853–859.

8 L. Zhao, C. Xu, H. Su, J. Liang, S. Lin, L. Gu, X. Wang, M. Chen and N. Zheng, *Adv. Sci.*, 2015, **2**, 1500–1505.

Open Access Article. Published on 18 June 2019. Downloaded on 5/2/2026 7:02:40 AM.
This article is licensed under a Creative Commons Attribution-NonCommercial 3.0 Unported Licence.

9 H. Kim, N. T. Khi, J. Yoon, H. Yang, Y. Chae, H. Baik, H. Lee, J. H. Sohn and K. Lee, *Chem. Commun.*, 2013, **49**, 2225–2227.
10 K. Jang, H. J. Kim and S. U. Son, *Chem. Adv. Mater.*, 2011, **22**, 1273–1275.
11 (*a*) Y. Zhang, M. E. Grass, J. N. Kuhn, F. Tao, S. E. Habas, W. Huang, P. Yang and G. A. Somorjai, *J. Am. Chem. Soc.*, 2008, **130**, 5868–5869; (*b*) S. Yao, Y. Yuan, C. Xiao, W. Z. Li, Y. Kou, P. J. Dyson and N. Yan, *J. Phys. Chem. C*, 2012, **116**, 15076–15086; (*c*) Y. Chen, Q. S. Chen, S. Y. Peng, Z. Q. Wang, G. Lu and G. C. Guo, *Chem. Commun.*, 2014, **50**, 1662–1664.
12 S. Choi, S. R. Lee, C. Ma, B. Oliy, M. Luo, M. Chi and Y. Xia, *ChemNanoMat*, 2016, **2**, 61–66.
13 H. Zhang, W. Li, M. Jin, J. Zeng, T. Yu, D. Yang and Y. Xia, *Nano Lett.*, 2011, **11**, 898–903.
14 S. Xie, H. Zhang, N. Lu, M. Jin, J. Wang, M. J. Kim, Z. Xie and Y. Xia, *Nano Lett.*, 2013, **13**, 6262–6268.
15 J. Park, J. Kim, Y. Yang, D. Yoon, H. Baik, S. Haam, H. Yang and K. Lee, *Adv. Sci.*, 2016, **3**, 1500252.
16 (*a*) J. D. Hoefelmeyer, K. Niesz, G. A. Somorja and T. D. Tilley, *Nano Lett.*, 2005, **5**, 435–438; (*b*) N. Zettsu, J. M. McLellan, B. Wiley, Y. Yin, Z. Y. Li and Y. Xia, *Angew. Chem., Int. Ed.*, 2006, **45**, 1288–1292; (*c*) S. M. Humphrey, M. E. Grass, S. E. Habas, K. Niesz, G. A. Somorjai and T. D. Tilley, *Nano Lett.*, 2007, **7**, 785–790; (*d*) H. Zhang, X. Xia, W. Li, J. Zeng, Y. Dai, D. Yang and Y. Xia, *Angew. Chem., Int. Ed.*, 2010, **49**, 5296–5300.
17 J. F. Moulder, W. F. Stickle, P. E. Sobol and K. D. Bomben, *Handbook of X-ray Photoelectron Spectroscopy*, Perkin-Elmer Co., Eden Prairie, MN, 1992.
18 L. Dai, Q. Chi, Y. Zhao, H. Liu, Z. Zhou, J. Li and T. Huang, *Mater. Res. Bull.*, 2014, **29**, 413–419.
19 H. Zhang, M. Jin and Y. Xia, *Angew. Chem., Int. Ed.*, 2012, **51**, 7656–7673.
20 (*a*) Y. Xiong, J. Chen, B. Wiley and Y. Xia, *J. Am. Chem. Soc.*, 2005, **127**, 7332–7333; (*b*) Y. Xiong, B. Wiley, J. Chen, Z.-Y. Li, Y. Yin and Y. Xia, *Angew. Chem., Int. Ed.*, 2005, **44**, 7913–7917.
21 (*a*) X. Xia and Y. Xia, *Nano Lett.*, 2012, **12**, 6038–6042; (*b*) K. D. Gilroy, H.-C. Peng, X. Yang, A. Ruditskiy and Y. Xia, *Chem. Commun.*, 2017, **53**, 4530–4541.

This journal is © The Royal Society of Chemistry 2019